Positron Emission Tomography and Near-Infrared Fluorescence Imaging of Vascular Endothelial Growth Factor with Dual-Labeled Bevacizumab

Yin Zhang,[1] Hao Hong,[2] Jonathan W. Engle,[1] Yunan Yang,[2] Todd E. Barnhart,[1] Weibo Cai[1,2,3,*]

[1] *Department of Medical Physics, University of Wisconsin - Madison, Madison, WI, USA*

[2] *Department of Radiology, University of Wisconsin - Madison, Madison, WI, USA*

[3] *University of Wisconsin Carbone Cancer Center, Madison, WI, USA*

Requests for reprints:

Weibo Cai, PhD, Departments of Radiology and Medical Physics, University of Wisconsin - Madison, Room 7137, 1111 Highland Ave, Madison, WI 53705-2275, USA

Email: wcai@uwhealth.org; Phone: 608-262-1749; Fax: 608- 265-0614

Abstract: The pivotal role of vascular endothelial growth factor (VEGF) in cancer is underscored by the approval of bevacizumab (Bev, a humanized anti-VEGF monoclonal antibody) for first line treatment of cancer patients. The aim of this study was to develop a dual-labeled Bev for both positron emission tomography (PET) and near-infrared fluorescence (NIRF) imaging of VEGF. Bev was conjugated to a NIRF dye (i.e. 800CW) and 2-S-(4-isothiocyanatobenzyl)-1,4,7-triazacyclononane-1,4,7-triacetic acid (p-SCN-Bn-NOTA) before ^{64}Cu-labeling. Flow cytometry analysis of U87MG human glioblastoma cells revealed no difference in VEGF binding affinity/specificity between Bev and NOTA-Bev-800CW. ^{64}Cu-labeling of NOTA-Bev-800CW was achieved with high yield. Serial PET imaging of U87MG tumor-bearing female nude mice revealed that tumor uptake of ^{64}Cu-NOTA-Bev-800CW was 4.6 ± 0.7, 16.3 ± 1.6, 18.1 ± 1.4 and 20.7 ± 3.7 %ID/g at 4, 24, 48 and 72 h post-injection respectively (n = 4), corroborated by in vivo/ex vivo NIRF imaging and biodistribution studies. Tumor uptake as measured by ex vivo NIRF imaging had a good linear correlation with the %ID/g values obtained from PET (R^2 = 0.93). Blocking experiments and histology both confirmed the VEGF specificity of ^{64}Cu-NOTA-Bev-800CW. The persistent, prominent, and VEGF-specific uptake of ^{64}Cu-NOTA-Bev-800CW in the tumor, observed by both PET and NIRF imaging, warrants further investigation and future clinical translation of such Bev-based imaging agents.

Introduction

One of the key requirements during tumor development is angiogenesis, the formation of new blood vessels, without which a tumor cannot grow beyond a few millimeters in diameter [1]. Over the last several decades, tremendous effort has been devoted to treating cancer by blocking the growth of new vessels that nourish tumors [2]. The vascular endothelial growth factor (VEGF)/VEGF receptor (VEGFR) signaling pathway plays a pivotal role in both normal vasculature development and many disease processes such as cancer [3]. VEGF-A is a homodimeric, disulfide-bound glycoprotein that exists in several isoforms with different numbers of amino acid residues (e.g. $VEGF_{121}$, $VEGF_{165}$, $VEGF_{189}$, and $VEGF_{206}$), as well as varying biological properties such as the ability to bind to cell surface heparin sulfate proteoglycans. The angiogenic actions of VEGF are mainly mediated via two endothelium-specific receptor tyrosine kinases, VEGFR-1 (Flt-1/FLT-1) and VEGFR-2 (Flk-1/KDR) [3].

The pivotal role of VEGF/VEGFR signaling pathway in cancer is underscored by the approval of a humanized anti-VEGF monoclonal antibody, bevacizumab (Avastin; Genentech), for first line treatment of cancer patients [4]. However, although bevacizumab (abbreviated as "Bev" in the remaining text) improves survival of colorectal and lung cancer patients when used in combination with chemotherapy [5, 6], the benefit and/or validity of such anti-angiogenic therapy is hotly debated in many other solid tumor types. For example, three large randomized prospective trials of unselected patients with metastatic breast cancer demonstrated that addition of Bev to

chemotherapy improves progression-free survival [7-9], which led to provisional approval by the Food and Drug Administration (FDA). However, meta-analyses of these trials showed that patients who received Bev did not survive longer than those who received placebo [10, 11]. Such lack of survival benefit ultimately led the FDA to begin revoking the approval in December 2010. Since cancer is a highly heterogeneous disease, one intriguing and likely explanation is that only lesions with high angiogenic activity will benefit from anti-angiogenic therapy.

The ultimate goal of 21st century personalized medicine in cancer patient management is to identify the right patient population for the right therapy at the right time, as well as to provide quantitative, non-invasive, and accurate information about the therapeutic responses in real-time. Development of a Bev-based imaging agent can play important roles in these aspects, as well as elucidating the function and modulation of VEGF/VEGFR signaling during cancer development/intervention. Positron emission tomography (PET), very sensitive (down to 10^{-12} molar) and quantitative with superb tissue penetration, has been widely used in clinical oncology for tumor staging and treatment monitoring, where ^{18}F-FDG was used as the tracer for measuring tumor glucose metabolism [12-15]. High resolution PET scanners continue to be developed and made available for imaging small animals, improving the capacity for in vivo studies in mice, primates, and humans. This will facilitate cross-species comparisons, which are critical for successful translational research studies and optimal benefit from research using experimental model systems.

To date, Bev has been labeled with a number of PET isotopes such as [89]Zr [16, 17], [124]I [18], [86]Y [19], and [64]Cu [20]. In addition, it has also been investigated with various other imaging techniques such as single photon emission computed tomography [21, 22], ultrasound [23], and optical imaging [24, 25]. To the best of our knowledge, no dual-labeled Bev has been reported yet for non-invasive imaging of VEGF with multiple modalities. In this study, we labeled Bev with both ^{64}Cu and a near-infrared fluorescent (NIRF) dye, IRDye 800CW (Ex: 778 nm; Em: 806 nm), and investigated the in vivo characteristics of the dual-labeled agent in a xenograft tumor model. Clinically, such a dual-modality PET/NIRF agent may be useful for lesion detection, patient selection, therapeutic response monitoring (all with PET), image-guided surgery (with NIRF), among others.

Materials and methods

Reagents

AlexaFluor488- and Cy3-labeled secondary antibodies were purchased from Jackson Immunoresearch Laboratories, Inc. (West Grove, CA). 2-S-(4-isothiocyanatobenzyl)-1,4,7-triazacyclononane-1,4,7-triacetic acid (p-SCN-Bn-NOTA) and Chelex 100 resin (50-100 mesh) were purchased from Macrocyclics, Inc. (Dallas, TX) and Sigma-Aldrich (St. Louis, MO), respectively. IRDye 800CW-NHS ester was acquired from LI-COR Biosciences Co. (Lincoln, NE). Water and all buffers were of Millipore grade and pre-treated with Chelex 100 resin to ensure that the aqueous solution was heavy metal-free.

PD-10 columns were purchased from GE Healthcare (Piscataway, NJ). All other reaction buffers and chemicals were from Thermo Fisher Scientific (Fair Lawn, NJ).

Cell line and animal model

U87MG human glioblastoma cells were purchased from the American Type Culture Collection (ATCC, Manassas, VA) and cultured in DMEM medium (Invitrogen, Carlsbad, CA) with 10% fetal bovine serum at 37 ºC with 5% CO_2. Cells were used for in vitro and in vivo experiments when they reached ~75% confluence. All animal studies were conducted under a protocol approved by the University of Wisconsin Institutional Animal Care and Use Committee. Four- to five-week-old female athymic nude mice were purchased from Harlan (Indianapolis, IN) and U87MG tumors were established by subcutaneously injecting 5×10^6 cells, suspended in 100 μL of 1:1 mixture of DMEM medium and Matrigel (BD Biosciences, Franklin lakes, NJ), into the front flank of mice. Tumor sizes were monitored every other day and mice were used for in vivo experiments when the diameter of tumors reached 5-8 mm.

Labeling of Bev

NOTA conjugation was carried out at pH 9.0, with the reaction ratio of p-SCN-Bn-NOTA:Bev being 25:1. Subsequently, NOTA-Bev was purified using PD-10 columns with phosphate-buffered saline (PBS) as the mobile phase. A molar ratio of 2:1 was used for the reaction between 800CW-NHS and NOTA-Bev at pH 8.5. After

continuously stirring the reaction mixture at room temperature (RT) for 2 h, NOTA-Bev-800CW was purified with PD-10 columns. ^{64}Cu-labeling of NOTA-Bev-800CW (25 µg per 37 MBq of ^{64}Cu) and tracer purification with PD-10 columns was carried out similar as described previously [26]. The radioactive fractions containing ^{64}Cu-NOTA-Bev-800CW were collected and passed through a 0.2 µm syringe filter for in vivo experiments.

Flow cytometry

The immunoreactivity of Bev and NOTA-Bev-800CW to U87MG cells were compared by fluorescence-activated cell sorting (FACS) analysis. Briefly, cells were harvested and suspended in cold PBS (pH 7.4) with 2% bovine serum albumin at a concentration of 5 × 10^6 cells/mL. The cells were incubated with various concentrations of Bev or NOTA-Bev-800CW (1 or 5 µg/mL) for 30 min at RT, washed three times with cold PBS, and centrifuged at 1,000 rpm for 5 min. After incubation with AlexaFluor488-labeled goat anti-human IgG (4 µg/mL) for 30 min at RT, the cells were washed and analyzed by FACS using a BD FACSCalibur 4-color analysis cytometer (Becton-Dickinson, San Jose, CA), which is equipped with 488 nm and 633 nm lasers and FlowJo analysis software (Tree Star, Inc., Ashland, OR).

Imaging and biodistribution studies

PET scans were performed using an Inveon microPET/microCT rodent model scanner

(Siemens Medical Solutions USA, Inc.). Each U87MG tumor-bearing mouse was intravenously injected with 5-10 MBq of ^{64}Cu-NOTA-Bev-800CW, adjusted to contain 300 picomoles (pmol) of 800CW using "cold" NOTA-Bev-800CW. Five-minute static PET scans were performed at various time points post-injection (p.i.). The images were reconstructed using a maximum a posteriori (MAP) algorithm, with no attenuation or scatter correction. Region-of-interest (ROI) analysis of each PET scan was performed using vendor software (Inveon Research Workplace [IRW]) on decay-corrected whole-body images as described previously [27], to calculate the percentage injected dose per gram of tissue (%ID/g) values for the U87MG tumor and several major organs. A subset of mice was also subjected to CT scans, with a voxel resolution of 210 μm. Fiducial markers were used for co-registration and images were reconstructed using the vendor software (Inveon Acquisition Workplace; Siemens). The CT and PET datasets were registered via rigid registration in IRW.

Immediately after PET scanning, the mice were imaged in an IVIS Spectrum scanner (Caliper, Hopkinton, MA) using the excitation filter of 745 nm and emission filter of 800 nm. All fluorescence images were acquired with 3 s exposure and longitudinal NIRF images for each mouse were displayed with common minimum and maximum values. Using vendor software, ROIs were drawn on the U87MG tumors and the average radiant efficiency (presented as mean ± SD in the unit of $[p/sec/cm^2/sr]/[\mu W/cm^2]$) within the ROI was used for subsequent quantitative analysis. Blocking studies were carried out to evaluate the VEGF specificity of ^{64}Cu-NOTA-Bev-800CW in vivo, where a group of 4 mice was each injected with 2 mg of Bev within 6 h before ^{64}Cu-NOTA-Bev-800CW

administration and subjected to serial PET/NIRF imaging as described above.

After the last in vivo PET/NIRF imaging at 72 h p.i., blood, U87MG tumor, and major organs/tissues were harvested and imaged ex vivo with both scanners to validate the in vivo findings. Biodistribution studies were also carried out to confirm that the quantitative tracer uptake values based on PET imaging truly represented the radioactivity distribution in tumor-bearing mice. Blood, U87MG tumor, and major organs/tissues were collected and wet-weighed. The radioactivity in each tissue was measured using a gamma-counter (Perkin Elmer) and presented as %ID/g. The U87MG tumor and mouse liver were also frozen and sectioned for histological analysis.

Histology

Frozen tissue slices of 5 μm thickness were fixed with cold acetone for 10 min and dried in the air for 30 min. After rinsing with PBS and blocking with 10% donkey serum for 30 min at RT, the slices were incubated with Bev (2 μg/mL) for 1 h at 4 °C and visualized using AlexaFluor488-labeled goat anti-human IgG. All images were acquired with a Nikon Eclipse Ti microscope.

Statistical analysis

Quantitative data were expressed as mean ± SD. Means were compared using Student's t-test. P values < 0.05 were considered statistically significant. The %ID/g

values based on PET were correlated with the quantitative data obtained from ex vivo NIRF imaging. Applying a linear fit, the correlation coefficient (R^2) was calculated to measure the strength of the association between the PET and ex vivo NIRF data. P values < 0.05 were considered to have a statistically significant linear correlation between the two measurements.

Results

In vitro investigation of NOTA-Bev-800CW

Based on UV measurements, there were ~5 NOTA and ~0.8 800CW conjugated to each Bev molecule. Since fluorescence resonance energy transfer only occurs when two fluorophores are within 10 nm (about the size of an antibody), less than one 800CW per Bev can avoid self-quenching due to close proximity of 800CW molecules, which allows for accurate measurement of 800CW concentration based on its fluorescence signal. Such minimal NOTA/800CW conjugation of Bev did not alter its VEGF binding affinity, and no observable differences were found between Bev and NOTA-Bev-800CW at 1 µg/mL or 5 µg/mL concentrations, as evidenced by FACS analysis using U87MG cells (**Figure 1**).

[64]Cu-labeling and PET imaging

[64]Cu-labeling and purification took 60 ± 10 min (n = 10). The decay-corrected

radiochemical yield was > 80%, based on 25 µg of NOTA-Bev-800CW per 37 MBq of ^{64}Cu, with a radiochemical purity of > 98%. The specific activity of ^{64}Cu-NOTA-Bev-800CW was about 1.1 GBq/mg protein, assuming complete recovery of the conjugate after size exclusion chromatography.

The time points of 4, 24, 48, and 72 h p.i. were chosen for serial PET/NIRF scans after intravenous injection of ^{64}Cu-NOTA-Bev-800CW. Coronal PET images that contain the U87MG tumors are shown in **Figure 2A**, with the quantitative data obtained from ROI analysis and representative PET/CT fused images of a mouse at 48 h p.i. shown in **Figure 3**. Similar as other ^{64}Cu-labeled antibodies which typically have long circulation half-lives [26, 28, 29], blood pool activity of ^{64}Cu-NOTA-Bev-800CW was prominent at early time points and gradually declined over time. The radioactivity in the blood was 20.5 ± 3.8, 17.9 ± 1.8, 14.3 ± 2.2 and 13.0 ± 2.8 %ID/g at 4, 24, 48 and 72 h p.i. respectively, while liver uptake of ^{64}Cu-NOTA-Bev-800CW was 14.4 ± 3.7, 17.2 ± 2.0, 13.8 ± 2.9 and 12.8 ± 2.7 %ID/g at 4, 24, 48 and 72 h p.i. respectively (n = 4; **Figure 3A**). The U87MG tumors were clearly visible by PET starting from 24 h p.i. (**Figure 2A**), with %ID/g values of 4.6 ± 0.7, 16.3 ± 1.6, 18.1 ± 1.4 and 20.7 ± 3.7 at 4, 24, 48 and 72 h p.i. respectively (n = 4; **Figure 3A**).

Administering a blocking dose of Bev six hours before ^{64}Cu-NOTA-Bev-800CW injection reduced the tumor uptake to very low level (< 7 %ID/g; P < 0.01 at 24, 48 and 72 h p.i. when compared with mice injected with ^{64}Cu-NOTA-Bev-800CW alone; **Figure 2A, 3B**), which clearly indicated VEGF specificity of the tracer in vivo. Radioactivity in the blood

was 23.6 ± 1.8, 13.4 ± 1.7, 11.2 ± 1.4 and 10.5 ± 1.0 %ID/g at 4, 24, 48 and 72 h p.i. respectively, whereas liver uptake was 17.8 ± 1.8, 14.3 ± 2.0, 13.1 ± 2.0 and 11.4 ± 1.7 %ID/g at 4, 24, 48 and 72 h p.i. respectively (n = 4; **Figure 3B**), both are similar to that of mice injected with ^{64}Cu-NOTA-Bev-800CW alone.

In vivo NIRF imaging

Serial in vivo NIRF imaging of U87MG tumor-bearing mice was carried out immediately after the PET scans, with representative images from each group shown in **Figure 2B**. Similar as PET findings, U87MG tumors were clearly visible starting from 24 h p.i. Quantitative ROI analysis yielded average tumor signal intensity of $1.20\times10^7 \pm 3.86\times10^6$, $1.92\times10^7 \pm 3.69\times10^6$, $1.52\times10^7 \pm 1.94\times10^6$ and $1.36\times10^7 \pm 3.94\times10^6$ [p/s/cm^2/sr]/[μW/cm^2] at 4, 24, 48 and 72 h p.i., respectively (n = 4; **Figure 4A**). Pre-injection of 2 mg of Bev per mouse before ^{64}Cu-NOTA-Bev-800CW administration resulted in tumor signal intensity of $1.28\times10^7 \pm 2.56\times10^6$, $1.16\times10^7 \pm 1.04\times10^6$, $8.93\times10^6 \pm 1.03\times10^6$ and $7.74\times10^6 \pm 1.00\times10^6$ [p/s/cm^2/sr]/[μW/cm^2] at 4, 24, 48 and 72 h p.i., respectively (n = 4; **Figure 4A**; P < 0.05 at 24, 48 and 72 h p.i. when compared to mice injected with ^{64}Cu-NOTA-Bev-800CW alone). Overall, the in vivo NIRF imaging results are in agreement with the PET findings, suggesting good stability of ^{64}Cu-NOTA-Bev-800CW in U87MG tumor-bearing mice.

Ex vivo studies

All mice were euthanized after the last PET scans at 72 h p.i. Major organs were subjected to both NIRF and PET imaging ex vivo (**Figure 4C**), which corroborated each other and are in accordance with the in vivo PET/NIRF results. Quantitative data from ROI analysis of major tissues, based on ex vivo NIRF imaging, are shown in **Figure 4B**. Excellent tumor contrast was observed in mice injected with ^{64}Cu-NOTA-Bev-800CW, but not in the blocking group. Linear correlation between the ex vivo NIRF data and %ID/g values based on PET, using a total of 8 data points (U87MG tumor at 72 h p.i. for two groups of mice with four mice per group), gave a statistically significant (P < 0.001) linear correlation with an R^2 value of 0.93 (**Figure 4D**) which indicates that NIRF imaging can give accurate quantitative results in ex vivo settings.

Biodistribution data at 72 h p.i. showed that U87MG tumor uptake of ^{64}Cu-NOTA-Bev-800CW was higher than that of all organs in mice (**Figure 5A**), thereby providing excellent contrast. Pre-injection of a blocking dose of Bev led to a significant decrease in tumor uptake of ^{64}Cu-NOTA-Bev-800CW (P < 0.05; n = 4), corroborating the in vivo PET findings and strongly suggested that tumor uptake of the tracer is VEGF-A mediated. Overall, the quantification results obtained from biodistribution studies and PET scans matched very well, confirming that quantitative ROI analysis of non-invasive PET scans truly reflected tracer distribution in vivo.

Fluorescence signal in the U87MG tumor, after immunofluorescence staining of VEGF, was quite heterogeneous, mainly from the tumor extracellular matrix (ECM) rather than the U87MG cells (**Figure 5B**). Such finding is in good agreement with other literature

reports [20, 25]. We believe that the fluorescence signal of VEGF staining is not from the tumor vasculature since Bev does not cross-react with murine VEGF [30]. VEGF staining of mouse liver gave very low signal, indicating that liver does not have significant level of VEGF. Thus, uptake of ^{64}Cu-NOTA-Bev-800CW in the liver was largely unrelated to target binding and more likely attributed to non-specific capture by the reticuloendothelial system (RES) and hepatic clearance of the tracer. Taken together, the ex vivo findings corroborated the in vivo data of ^{64}Cu-NOTA-Bev-800CW, warranting further investigation and applications of this tracer.

Discussion

The goal of this study was to develop a VEGF-specific tracer for both PET and NIRF imaging, which was successfully achieved by labeling Bev with both ^{64}Cu and the NIRF dye 800CW. U87MG human glioblastoma cells were used here for in vitro characterization of NOTA-Bev-800CW to confirm its VEGF-binding affinity/specificity. It has been shown that U87MG cells express three isoforms of VEGF-A, namely VEGF$_{121}$, VEGF$_{165}$, and VEGF$_{189}$ at similar levels [31]. Among the at least seven isoforms of VEGF-A, VEGF$_{121}$ is freely soluble while all VEGF$_{189}$ is bound to the cell membrane or ECM [32]. VEGF$_{165}$ exhibits an intermediary behavior (i.e. partly diffusible and partly bound). Since only membrane-bound VEGF can be detected by FACS analysis of Bev and NOTA-Bev-800CW, the fluorescence signal of U87MG cells was not very strong. Nonetheless, no difference between NOTA-Bev-800CW and Bev was

observed in FACS analysis, clearly demonstrating that NOTA/800CW conjugation of Bev did not affect its VEGF binding affinity.

In animal studies, good tumor uptake was observed for ^{64}Cu-NOTA-Bev-800CW, which may be partly attributed to the high local concentration of (soluble) VEGFs at the tumor site. One major difference between the in vivo studies and FACS analysis of U87MG cells is that the imaging targets of ^{64}Cu-NOTA-Bev-800CW are all VEGF isoforms, not only those on U87MG cells and the ECM but also soluble VEGF in the tumor local environment, whereas only membrane-bound VEGF isoforms are detected in FACS studies.

ROI analysis of the PET data showed that ^{64}Cu-NOTA-Bev-800CW uptake in the tumor kept increasing at late time points (**Figure 3A**), while in vivo NIRF imaging gave a decreasing trend of tumor uptake over time (**Figure 4A**). Such an interesting finding may be due to degradation of the tracer over time and subsequent efflux of 800CW-containing species from the tumor, whereas ^{64}Cu is more readily trapped inside the tumor (cells) like many other radiometals such as ^{111}In and ^{89}Zr [16, 21]. Another contributing factor to such observation may be that a portion of 800CW molecules lose the fluorescence if degraded or photobleached, which is not the case for ^{64}Cu detection (all quantitative data for PET were decayed-corrected). Nevertheless, there is still a good linear correlation between the in vivo PET data (%ID/g) and ex vivo NIRF quantification (radiant efficiency) at 72 h p.i., suggesting that NIRF imaging can allow for relatively accurate quantification of tracer uptake ex vivo (and to a certain degree also in

superficial tissues in vivo). However, the accuracy of quantification is much lower for deeper tissues of darker color, as can be seen for the liver in both in vivo and ex vivo NIRF imaging. In clinical settings, NIRF imaging can be used for imaging tissues close to the surface of the skin (e.g. breast cancer imaging), tissues accessible by endoscopy (such as malignant lesions in the esophagus and colon), and intraoperative visualization (i.e. image-guided surgery).

Guiding surgery with molecularly targeted fluorescent agents has attracted enormous interest over the last decade. Recently, a proof-of-principle study investigating the potential benefit of intraoperative tumor-specific fluorescence imaging in staging and debulking surgery for ovarian cancer using a systemically administered targeted fluorescent agent (folate-FITC, which emits in the visible range) was reported [33]. The use of a NIRF agent, which has much better signal penetration in an imaging window with significantly less autofluorescence than in the visible range, is more desirable for surgery guidance with the development of suitable intraoperative imaging systems. The incorporation of two imaging labels on a single targeting ligand, where both labels were conjugated at a minimal level thereby exhibiting no detectable effect on the antigen binding affinity/specificity as demonstrated in our study, is advantageous than single modality imaging from regulatory perspectives. The need for comprehensive toxicity/dosimetry studies in multiple animal species for one agent instead of two separate agents (one for each imaging modality) can significantly reduce the development cost and facilitate future clinical translation of novel imaging agents.

Over the last decade, imaging of VEGFR expression has gained enormous interest not only in cancer but also in many other angiogenesis-related diseases [34-44]. Due to the soluble and dynamic nature of VEGF proteins, imaging VEGF expression is much more challenging than imaging VEGFR expression and it has not been well studied. Besides Bev, a few other radiolabeled anti-VEGF antibodies have also been reported previously such as [124]I-labeled VG76e [45] and HuMV833 [46]. Phase I trial of the latter revealed that antibody distribution and clearance was quite heterogeneous, not only between and within patients but also between and within individual tumors, which underscored the importance of patient selection to achieve maximum therapeutic effect. Imaging VEGF and VEGFR expression are both important for cancer diagnosis and monitoring the therapeutic efficacy of anti-angiogenic therapies. Examining the tumor in the same animals or cancer patients with both VEGF- and VEGFR-targeted tracers may give important insights about the expression kinetics of VEGF and VEGFRs during cancer development and cancer therapy.

In conclusion, herein we report the development, characterization, and in vivo investigation of a dual-labeled Bev (with ^{64}Cu and a NIRF dye 800CW) for both PET and NIRF imaging of VEGF in a xenograft tumor model. Persistent, prominent and VEGF-specific uptake of ^{64}Cu-NOTA-Bev-800CW in the U87MG tumor was observed with both imaging modalities, which was validated by various in vitro, in vivo, and ex vivo studies. Upon further optimization and development, such dual-labeled PET/NIRF agents can be translated into the clinic for many applications such as disease diagnosis, patient stratification, treatment monitoring, image-guided surgery, etc.

Acknowledgment

References

[1]   Folkman J. Tumor angiogenesis: therapeutic implications. N Engl J Med 1971; 285: 1182-1186.

[2]   Folkman J. Angiogenesis: an organizing principle for drug discovery? Nat Rev Drug Discov 2007; 6: 273-286.

[3]   Ferrara N. Vascular endothelial growth factor: basic science and clinical progress. Endocr Rev 2004; 25: 581-611.

[4]   Ferrara N, Hillan KJ, Gerber HP and Novotny W. Discovery and development of bevacizumab, an anti-VEGF antibody for treating cancer. Nat Rev Drug Discov 2004; 3: 391-400.

[5]   Hurwitz H, Fehrenbacher L, Novotny W, Cartwright T, Hainsworth J, Heim W, Berlin J, Baron A, Griffing S, Holmgren E, Ferrara N, Fyfe G, Rogers B, Ross R and Kabbinavar F. Bevacizumab plus irinotecan, fluorouracil, and leucovorin for metastatic colorectal cancer. N Engl J Med 2004; 350: 2335-2342.

[6]   Sandler A, Gray R, Perry MC, Brahmer J, Schiller JH, Dowlati A, Lilenbaum R and Johnson DH. Paclitaxel-carboplatin alone or with bevacizumab for non-small-cell lung cancer. N Engl J Med 2006; 355: 2542-2550.

[7]   Miles DW, Chan A, Dirix LY, Cortes J, Pivot X, Tomczak P, Delozier T, Sohn JH, Provencher L, Puglisi F, Harbeck N, Steger GG, Schneeweiss A, Wardley AM, Chlistalla A and Romieu G. Phase III study of bevacizumab plus docetaxel compared with placebo plus docetaxel for the first-line treatment of human epidermal growth factor receptor 2-negative metastatic breast cancer. J Clin Oncol 2010; 28: 3239-3247.

[8]   Robert NJ, Dieras V, Glaspy J, Brufsky AM, Bondarenko I, Lipatov ON, Perez EA, Yardley DA, Chan SY, Zhou X, Phan SC and O'Shaughnessy J. RIBBON-1: randomized, double-blind, placebo-controlled, phase III trial of chemotherapy with or without bevacizumab for first-line treatment of human epidermal growth factor receptor 2-negative, locally recurrent or metastatic breast cancer. J Clin Oncol 2011; 29: 1252-1260.

[9]   Miller K, Wang M, Gralow J, Dickler M, Cobleigh M, Perez EA, Shenkier T, Cella D and Davidson NE. Paclitaxel plus bevacizumab versus paclitaxel alone for metastatic breast cancer. N Engl J Med 2007; 357: 2666-2676.

[10]   Valachis A, Polyzos NP, Patsopoulos NA, Georgoulias V, Mavroudis D and Mauri D. Bevacizumab in metastatic breast cancer: a meta-analysis of randomized controlled trials. Breast Cancer Res Treat 2010; 122: 1-7.

[11]   Pivot X, Schneeweiss A, Verma S, Thomssen C, Passos-Coelho JL, Benedetti G, Ciruelos E, von Moos R, Chang HT, Duenne AA and Miles DW. Efficacy and safety of bevacizumab in combination with docetaxel for the first-line treatment of elderly patients with locally recurrent or metastatic breast cancer: Results from AVADO. Eur J Cancer 2011; 47: 2387-2395.

[12]   Vach W, Høilund-Carlsen PF, Fischer BM, Gerke O and Weber W. How to study optimal timing of PET/CT for monitoring of cancer treatment. Am J Nucl Med Mol Imaging 2011; 1: 54-62.

[13]   Rakheja R, Ciarallo A, Alabed YZ and Hickeson M. Intravenous administration of diazepam significantly reduces brown fat activity on ^{18}F-FDG PET/CT. Am J Nucl Med Mol Imaging 2011; 1: 29-35.

[14]   Eary JF, Hawkins DS, Rodler ET and Conrad EUI. ^{18}F-FDG PET in sarcoma treatment response imaging. Am J Nucl Med Mol Imaging 2011; 1: 47-53.

[15]   Iagaru A. ^{18}F-FDG PET/CT: timing for evaluation of response to therapy remains a clinical challenge. Am J Nucl Med Mol Imaging 2011; 1: 63-64.

[16]   Nagengast WB, de Vries EG, Hospers GA, Mulder NH, de Jong JR, Hollema H, Brouwers AH, van Dongen GA, Perk LR and Lub-de Hooge MN. In vivo VEGF imaging with radiolabeled bevacizumab in a human ovarian tumor xenograft. J Nucl Med 2007; 48: 1313-1319.

[17]   Nagengast WB, de Korte MA, Oude Munnink TH, Timmer-Bosscha H, den Dunnen WF, Hollema H, de Jong JR, Jensen MR, Quadt C, Garcia-Echeverria C, van Dongen GA, Lub-de Hooge MN, Schroder CP and de Vries EG. [89]Zr-bevacizumab PET of early antiangiogenic tumor response to treatment with HSP90 inhibitor NVP-AUY922. J Nucl Med 2010; 51: 761-767.

[18]   Christoforidis JB, Carlton MM, Knopp MV and Hinkle GH. PET/CT imaging of I-124-radiolabeled bevacizumab and ranibizumab after intravitreal injection in a rabbit model. Invest Ophthalmol Vis Sci 2011; 52: 5899-5903.

[19]   Nayak TK, Garmestani K, Baidoo KE, Milenic DE and Brechbiel MW. PET imaging of tumor angiogenesis in mice with VEGF-A-targeted [86]Y-CHX-A''-DTPA-bevacizumab. Int J Cancer 2011; 128: 920-926.

[20]   Paudyal B, Paudyal P, Oriuchi N, Hanaoka H, Tominaga H and Endo K. Positron emission tomography imaging and biodistribution of vascular endothelial growth factor with ^{64}Cu-labeled bevacizumab in colorectal cancer xenografts. Cancer Sci 2011; 102: 117-121.

[21]   Stollman TH, Scheer MG, Leenders WP, Verrijp KC, Soede AC, Oyen WJ, Ruers TJ and Boerman OC. Specific imaging of VEGF-A expression with radiolabeled anti-VEGF monoclonal antibody. Int J Cancer 2008; 122: 2310-2314.

[22]   Nagengast WB, Hooge MN, van Straten EM, Kruijff S, Brouwers AH, den Dunnen WF, de Jong JR, Hollema H, Dierckx RA, Mulder NH, de Vries EG, Hoekstra HJ

and Hospers GA. VEGF-SPECT with ^{111}In-bevacizumab in stage III/IV melanoma patients. Eur J Cancer 2011; 47: 1595-1602.

[23]   Zhang L, Xu JS, Sanders VM, Letson AD, Roberts CJ and Xu RX. Multifunctional microbubbles for image-guided antivascular endothelial growth factor therapy. J Biomed Opt 2010; 15: 030515.

[24]   Withrow KP, Newman JR, Skipper JB, Gleysteen JP, Magnuson JS, Zinn K and Rosenthal EL. Assessment of bevacizumab conjugated to Cy5.5 for detection of head and neck cancer xenografts. Technol Cancer Res Treat 2008; 7: 61-66.

[25]   Terwisscha van Scheltinga AG, van Dam GM, Nagengast WB, Ntziachristos V, Hollema H, Herek JL, Schroder CP, Kosterink JG, Lub-de Hoog MN and de Vries EG. Intraoperative near-infrared fluorescence tumor imaging with vascular endothelial growth factor and human epidermal growth factor receptor 2 targeting antibodies. J Nucl Med 2011; 52: 1778-1785.

[26]   Hong H, Yang Y, Zhang Y, Engle JW, Barnhart TE, Nickles RJ, Leigh BR and Cai W. Positron emission tomography imaging of CD105 expression during tumor angiogenesis. Eur J Nucl Med Mol Imaging 2011; 38: 1335-1343.

[27]   Hong H, Severin GW, Yang Y, Engle JW, Zhang Y, Barnhart TE, Liu G, Leigh BR, Nickles RJ and Cai W. Positron emission tomography imaging of CD105 expression with [89]Zr-Df-TRC105. Eur J Nucl Med Mol Imaging 2011; Epub.

[28]   Cai W, Ebrahimnejad A, Chen K, Cao Q, Li ZB, Tice DA and Chen X. Quantitative radioimmunoPET imaging of EphA2 in tumor-bearing mice. Eur J Nucl Med Mol Imaging 2007; 34: 2024-2036.

[29]   Cai W, Wu Y, Chen K, Cao Q, Tice DA and Chen X. *In vitro* and *in vivo* characterization of ^{64}Cu-labeled Abegrin[TM], a humanized monoclonal antibody against integrin $a_v b_3$. Cancer Res 2006; 66: 9673-9681.

[30]   Yu L, Wu X, Cheng Z, Lee CV, LeCouter J, Campa C, Fuh G, Lowman H and Ferrara N. Interaction between bevacizumab and murine VEGF-A: a reassessment. Invest Ophthalmol Vis Sci 2008; 49: 522-527.

[31]   Cheng SY, Nagane M, Huang HS and Cavenee WK. Intracerebral tumor-associated hemorrhage caused by overexpression of the vascular endothelial growth factor isoforms $VEGF_{121}$ and $VEGF_{165}$ but not $VEGF_{189}$. Proc Natl Acad Sci USA 1997; 94: 12081-12087.

[32]   Houck KA, Leung DW, Rowland AM, Winer J and Ferrara N. Dual regulation of vascular endothelial growth factor bioavailability by genetic and proteolytic mechanisms. J Biol Chem 1992; 267: 26031-26037.

[33]   van Dam GM, Themelis G, Crane LM, Harlaar NJ, Pleijhuis RG, Kelder W, Sarantopoulos A, de Jong JS, Arts HJ, van der Zee AG, Bart J, Low PS and Ntziachristos V. Intraoperative tumor-specific fluorescence imaging in ovarian cancer by folate receptor-alpha targeting: first in-human results. Nat Med 2011; 17: 1315-1319.

[34]   Chan C, Sandhu J, Guha A, Scollard DA, Wang J, Chen P, Bai K, Lee L and Reilly RM. A human transferrin-vascular endothelial growth factor (hnTf-VEGF) fusion protein containing an integrated binding site for ^{111}In for imaging tumor angiogenesis. J Nucl Med 2005; 46: 1745-1752.

[35]   Blankenberg FG, Mandl S, Cao YA, O'Connell-Rodwell C, Contag C, Mari C, Gaynutdinov TI, Vanderheyden JL, Backer MV and Backer JM. Tumor imaging

using a standardized radiolabeled adapter protein docked to vascular endothelial growth factor. J Nucl Med 2004; 45: 1373-1380.

[36]   Backer MV, Levashova Z, Patel V, Jehning BT, Claffey K, Blankenberg FG and Backer JM. Molecular imaging of VEGF receptors in angiogenic vasculature with single-chain VEGF-based probes. Nat Med 2007; 13: 504-509.

[37]   Cai W and Chen X. Multimodality imaging of vascular endothelial growth factor and vascular endothelial growth factor receptor expression. Front Biosci 2007; 12: 4267-4279.

[38]   Cai W and Chen X. Multimodality molecular imaging of tumor angiogenesis. J Nucl Med 2008; 49 Suppl 2: 113S-128S.

[39]   Cai W, Chen K, Mohamedali KA, Cao Q, Gambhir SS, Rosenblum MG and Chen X. PET of vascular endothelial growth factor receptor expression. J Nucl Med 2006; 47: 2048-2056.

[40]   Wang H, Cai W, Chen K, Li ZB, Kashefi A, He L and Chen X. A new PET tracer specific for vascular endothelial growth factor receptor 2. Eur J Nucl Med Mol Imaging 2007; 34: 2001-2010.

[41]   Cai W, Guzman R, Hsu AR, Wang H, Chen K, Sun G, Gera A, Choi R, Bliss T, He L, Li ZB, Maag AL, Hori N, Zhao H, Moseley M, Steinberg GK and Chen X. Positron emission tomography imaging of poststroke angiogenesis. Stroke 2009; 40: 270-277.

[42]   Rodriguez-Porcel M, Cai W, Gheysens O, Chen IY, Chen K, He L, Willman JK, Wu JC, Li ZB, Mohamedali KA, Rosenblum MG, Chen X and Gambhir SS. Imaging of VEGF receptor in a rat myocardial infarction model using positron emission tomography. J Nucl Med 2008; 49: 667-673.

[43]   Willmann JK, Chen K, Wang H, Paulmurugan R, Rollins M, Cai W, Wang DS, Chen IY, Gheysens O, Rodriguez-Porcel M, Chen X and Gambhir SS. Monitoring of the biologic response to murine hindlimb ischemia using ^{64}Cu-labeled vascular endothelial growth factor-121 positron emission tomography. Circulation 2008; 117: 915-922.

[44]   Hao G, Hajibeigi A, De León-Rodríguez LM, Öz OK and Sun X. Peptoid-based PET imaging of vascular endothelial growth factor receptor (VEGFR) expression. Am J Nucl Med Mol Imaging 2011; 1: 65-75.

[45]   Collingridge DR, Carroll VA, Glaser M, Aboagye EO, Osman S, Hutchinson OC, Barthel H, Luthra SK, Brady F, Bicknell R, Price P and Harris AL. The development of [[124]I]iodinated-VG76e: a novel tracer for imaging vascular endothelial growth factor *in vivo* using positron emission tomography. Cancer Res 2002; 62: 5912-5919.

[46]   Jayson GC, Zweit J, Jackson A, Mulatero C, Julyan P, Ranson M, Broughton L, Wagstaff J, Hakannson L, Groenewegen G, Bailey J, Smith N, Hastings D, Lawrance J, Haroon H, Ward T, McGown AT, Tang M, Levitt D, Marreaud S, Lehmann FF, Herold M and Zwierzina H. Molecular imaging and biological evaluation of HuMV833 anti-VEGF antibody: implications for trial design of antiangiogenic antibodies. J Natl Cancer Inst 2002; 94: 1484-1493.

Figure Legends

Figure 1. Flow cytometry analysis of Bev and NOTA-Bev-800CW in U87MG human glioblastoma cells at different concentrations. Data from various control experiments are also shown.
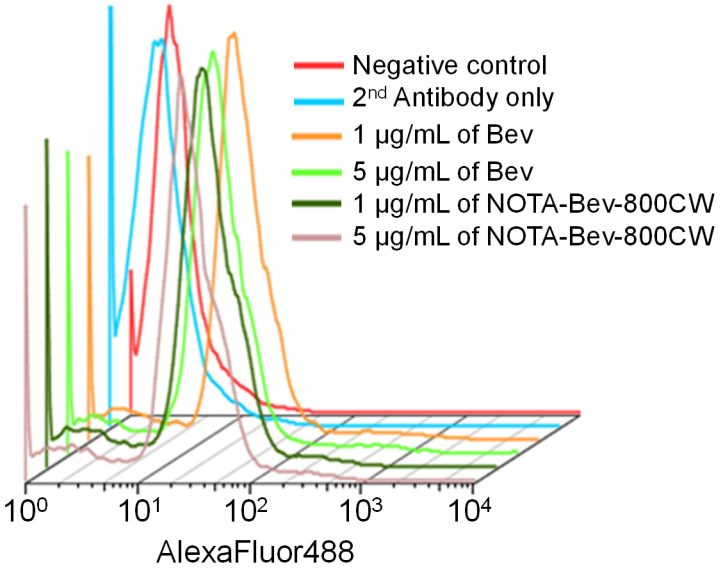
Figure 2. Serial in vivo PET/NIRF imaging of U87MG tumor-bearing mice. (**A**) Serial coronal PET images at 4, 24, 48 and 72 h post-injection of ^{64}Cu-NOTA-Bev-800CW, or 2 mg of Bev before ^{64}Cu-NOTA-Bev-800CW (i.e. blocking). (**B**) Serial NIRF images of the same mice in (**A**). The amount of 800CW injected into each mouse was ~300 pmol and images are representative of a group of 4 mice each. All images were acquired under the same condition and displayed at the same scale. Arrowheads indicate the U87MG tumors.

Figure 3. Quantitative analysis of the PET data. (**A**) Time-activity curves of the blood, liver, U87MG tumor, and muscle upon intravenous injection of ^{64}Cu-NOTA-Bev-800CW into tumor-bearing mice (n = 4). (**B**) Time-activity curves of the blood, liver, U87MG tumor, and muscle upon intravenous injection of ^{64}Cu-NOTA-Bev-800CW, after a blocking dose of Bev, into tumor-bearing mice (n = 4). (**C**) Representative PET/CT images of a U87MG tumor-bearing mouse at 48 h post-injection of ^{64}Cu-NOTA-Bev-800CW. Arrowheads indicate the tumor.

Figure 4. Ex vivo NIRF imaging and correlation with PET. (**A**) Signal intensity of the

U87MG tumor in the two groups of mice, based on in vivo NIRF imaging. (**B**) Signal intensity of the U87MG tumor and major organs in the two groups of mice, based on ex vivo NIRF imaging at 72 h post-injection. (**C**) Ex vivo NIRF and PET imaging of the U87MG tumor and major organs in the two groups at 72 h post-injection. Images are representative of 4 mice per group. T: U87MG tumor, L1: liver, B1: blood, H: heart, K: kidney, B2: bone, L2: lung, S: spleen, M: muscle. (**D**) Correlation of the ex vivo NIRF signal intensity in all U87MG tumor-bearing mice at 72 h post-injection with the %ID/g values based on ROI analysis of the PET data.

Figure 5. Biodistribution and histology studies. (**A**) Biodistribution data at 72 h post-injection of ^{64}Cu-NOTA-Bev-800CW, or 2 mg of Bev before ^{64}Cu-NOTA-Bev-800CW (i.e. blocking). *: $P < 0.05$ (n = 4). (**B**) Immunofluorescence VEGF staining of the U87MG tumor and liver tissue sections. Bev and AlexaFluor488-labeled goat anti-human IgG were used for VEGF staining. Images were acquired under the same condition and displayed at the same scale. Magnification: 200×.

Negative control
2nd Antibody only
1 μg/mL of Bev
5 μg/mL of Bev
1 μg/mL of NOTA-Bev-800CW
5 μg/mL of NOTA-Bev-800CW

10^0 10^1 10^2 10^3 10^4

AlexaFluor488

A

^{64}Cu-NOTA-Bev-800CW

^{64}Cu-NOTA-Bev-800CW + Blocking

25 % ID/g

0 % ID/g

4 h   24 h   48 h   72 h

B

^{64}Cu-NOTA-Bev-800CW

^{64}Cu-NOTA-Bev-800CW + Blocking

$\times 10^7 \dfrac{p/sec/cm^2/sr}{\mu W/cm^2}$

4.0

3.0

2.0

1.0

4 h   24 h   48 h   72 h

A ^{64}Cu-NOTA-Bev-800CW

B ^{64}Cu-NOTA-Bev-800CW + Blocking

C CT — PET — PET/CT

A — U87MG Tumor Radiance Efficiency ([p/s/cm²/sr]/[μW/cm²]) vs Post-injection Time
- ■ ^{64}Cu-NOTA-Bev-800CW
- ● ^{64}Cu-NOTA-Bev-800CW + Blocking

B — Radiance Efficiency ([p/s/cm²/sr]/[μW/cm²]) for Tumor, Liver, Blood, Heart, Kidney, Bone, Lung, Spleen, Muscle
- ■ ^{64}Cu-NOTA-Bev-800CW
- ▨ ^{64}Cu-NOTA-Bev-800CW + Blocking

C — ^{64}Cu-NOTA-Bev-800CW | ^{64}Cu-NOTA-Bev-800CW + Blocking
NIRF / PET

D — U87MG Tumor Radiance Efficiency ([p/s/cm²/sr]/[μW/cm²]) vs Tumor Uptake (%ID/g)
$R^2 = 0.93$
$P < 0.001$

A

B

U87MG Tumor   Liver